RSC Advances

PAPER

View Article Online
View Journal | View Issue

Cite this: *RSC Adv.*, 2025, **15**, 31162

Betel leaf-mediated zinc oxide nanoparticle-coated silk fibres: a sustainable approach for biomedical applications

Prakruthi Kanalli, Rohan R. Kundapur and Manu M. Joseph *

Clinical management of surgical site infections remains a challenge in biomedicine, where novel wound dressing materials are tested with a plethora of features. Here we describe a green and sustainable route to prepare biogenic zinc oxide nanoparticles (BZnONPs) using *Piper betle* leaf extract, which acts as a green reducing and stabilising agent. These biosynthesised nanoparticles were then used for the functional coating of degummed *Bombyx mori* silk fibers. Physico-chemical characterisation supports the efficient synthesis of crystalline, nanosized, and colloidal stable BZnONPs. The functionalization of silk fibers with BZnONPs resulted in the enhancement of the mechanical properties, tensile strength, and elasticity. Antibacterial testing proved the capability of the functional fibers against the strain *Staphylococcus aureus*. The as-synthesised fibers were biocompatible towards normal blood components, normal cells and exhibited slight toxicity toward cancer cells. Enhanced mechanical properties, antimicrobial action, and biocompatibility make BZnONP-coated silk fibers a leading player in various advanced biomedical devices, including sutures, wound dressings, tissue engineering scaffolds, and localised therapeutic platforms. Hence, this green nanotechnology approach opens up an alternative pathway toward the fabrication of multifunctional biomaterials with high translational value.

Received 22nd May 2025
Accepted 22nd August 2025

DOI: 10.1039/d5ra03600c

rsc.li/rsc-advances

1. Introduction

Almost 30 days post-operation, surgical site infections (SSIs) often come up. When implants are being placed, redness, swelling, and discharge could characterise these infections. These are superficial, affecting just the skin or could go deeper, involving subcutaneous tissues or structures. Such complications can also make their way back through recurrence, so there is definitely a need to find better means of combating antimicrobial resistance mechanisms.[1,2] Usually, the microorganisms that cause surgical site infections are from the patient's skin or mucosal flora. Surgical breach of these barriers provides a channel for pathogens, especially *Staphylococcus* species and methicillin-resistant *Staphylococcus aureus* (MRSA), into deeper tissues. Surgical procedures within the gastrointestinal tract may also introduce Gram-negative organisms like *Escherichia coli*, further complicating infection control. The use of antimicrobial sutures has attracted much interest and research for preventing bacterial colonisation at the wound site.[3,4] widely used would be silk among suture materials, given its perfect knot strength, flexibility, easy handling, and biocompatibility. However, it could be contaminated by microbes, which limits its use in settings where infection may develop.[5] Of all suture materials, silk has been a long-standing favourite because of its superior knot strength, flexibility, ease of handling, and excellent biocompatibility.[6–8] This study pertains to the generation of ZnO nanoparticles (ZnO NPs) and ZnO NPs-coated silk fibres to develop such infection-resistant biomaterials for surgery and wound-care applications.

Considered a natural biopolymer, silk fibroin is frequently employed in tissue engineering because of its strength, biodegradability, lack of antigenicity, and biocompatibility. When converted into fibers, it translates into strength and elasticity imperative for suture material, bone repair, ligament regeneration, and vascular grafts. The silk fibroin matrix allows cells to adhere and proliferate. The properties of silk can be modified, but the retention of moisture by silk can encourage microbial attack, and thus, improving the antimicrobial nature of silk becomes critical. These antimicrobial modifications should be able to keep infection at bay without damaging the structural integrity of the silk.[9,10] Among emerging trends in this direction have been the use of natural antimicrobial agents.[11] Metallic nanoparticles (NPs), particularly zinc and silver NPs, have been recognised as having strong, broad-spectrum antimicrobial activity, providing prospects to combat drug-resistant pathogens.[12,13] By bringing about an environment unfavourable for microbial growth, the incorporation of such NPs into suture materials would be well-suited in maintaining the mechanical properties and handling of the sutures.[14] NPs are gaining attention from several areas because of their unique optical, electrical, catalytic, and magnetic properties.[15] Among these,

Department of Life Sciences, CHRIST University, Bengaluru – 560029, Karnataka, India. E-mail: manu.joseph@christuniversity.in; manumjoseph2000@gmail.com

ZnO NPs have been marked out concerning their long history as well as their present use in medicines and cosmetics, from ointments for wounds and sunscreens to antimicrobial coatings on medical devices. With growing ecological concerns, even though environmentally friendly, green synthesis of ZnO NPs is considered for reducing environmental footprints without compromising functional effectiveness for their potential medical applications.[16,17]

Piper betle, belonging to the Piperaceae family, is a plant that can be tapped into green synthesis because of its many therapeutic attributes and richness with phytochemicals. This plant is indigenously grown and distributed widely in South and Southeast Asian countries. *Piper betle* is part of traditional medicine and has already long in use for centuries until now.[18] According to findings from many studies, extracts from *Piper betle* have been shown to be very effective in antioxidant, antimicrobial, anti-inflammatory, and anticancer properties.[19,20] *Piper betle* leaf, commonly called betel leaf or "paan," holds cultural and medicinal value in India. Used for centuries in Ayurveda and traditional healing, it is highly valued for its antiseptic, digestive, and stimulating properties. Betel leaves are often chewed with areca nut and slaked lime, which promote oral well-being and appetite. Medicinally, they have been used to treat respiratory ailments, wounds, and inflammation, and applied topically for their soothing properties. Besides therapeutic use, betel leaves also find important use in religious rituals and social customs across India.[21,22]

The antibacterial and anti-inflammatory activities of *Piper betle* extracts suggest an exciting potential for the development of high-performing natural antimicrobials. These properties are useful for the application of NPs formulation for bioactive, biocompatible materials to fight against microbial infection and inhibition of inflammation, as well as oxidative stress. The green synthesis of NPs using *Piper betle* gives a dual advantage as it can fit the role of both reducing and stabilising agents for the biogenesis of NPs. Moreover, the resultant NPs can be imparted with bifunctional characteristics according to the natural medicinal constituents of the leaf extract. Thus, this synergistic approach of synthesis is not only an environmentally benign methodology but also complements therapy in efficacy towards its downstream nanomaterials. Bio-synthesised silver NPs from *Piper betle* leaf extract served as excellent antimicrobial agents when coated over pig leather[23] and demonstrated antifungal activity against plant-pathogenic fungi,[24] whereas copper NPs were superior antibacterial compounds and even served to be used for the removal of pharmaceutical compounds such as Atorvastatin.[25] However, *Piper betle* leaf extract was not documented for the bio-fabrication of ZnO NPs, and hence, we thought of making use of this untapped niche in the current manuscript. Silk fibers were carefully prepared and coated with

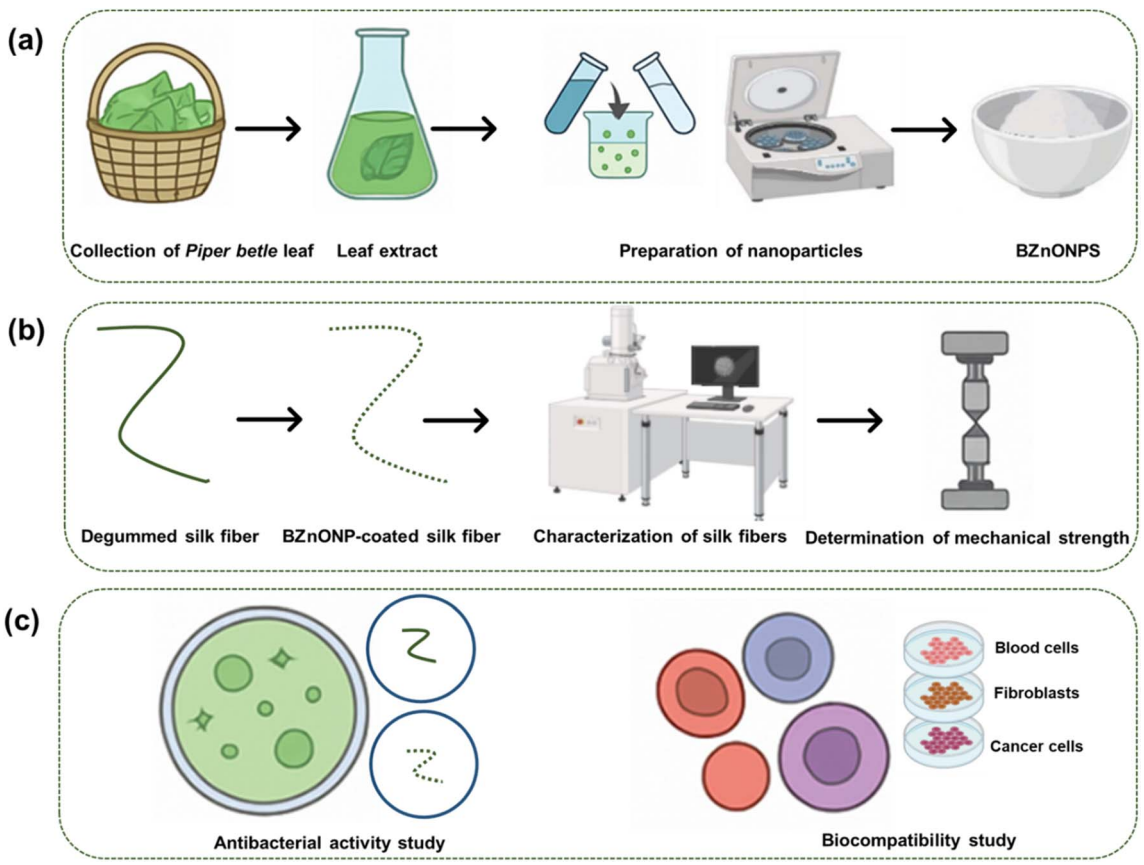

Fig. 1 Schematic illustration of the (a) synthesis of ZnO NPs using *Piper betle* leaf extract. (b) Process involved in the fabrication, characterisation of BZnONP-coated silk fibres and testing of mechanical strength. (c) Functional evaluation of the coated silk fibres for biomedical applications. Prepared using BioRender software.

biogenic ZnO NPs capped with *Piper betle* leaf extract. We envision that the ZnO NPs-coated silk fibres can be developed as infection-resistant biomaterials for surgery and wound-care applications (Fig. 1).

Silk is extensively recognised for its exceptional mechanical properties and biocompatibility. However, its high moisture retention and nutrient-absorbing capacity can create a favourable microenvironment to attract bacterial growth. To overcome this limitation, we synthesized biogenic zinc oxide nanoparticles (BZnONPs) using *Piper betle* leaf extract and used them to functionalize degummed *Bombyx mori* silk fibers. A complete set of characterisations was then performed on the in-house fabrication, including spectroscopic, physicochemical, mechanical, and biological assays. These BZnONPs functionalized fibers were then tested for antibacterial activity against *Staphylococcus aureus*, mechanical strength, biocompatibility with blood components, and human cells. These findings demonstrated the enhanced mechanical performance, excellent antibacterial activity, and high biocompatibility, indicating that the NP-coating strategy holds promising prospects to be used in biomedical applications.

2. Materials and methods

2.1 Collection and preparation of *Piper betle* leaf extract

Fresh *Piper betle* (betel) leaves were harvested from Demlapura village, Thirthahalli, Karnataka, India (latitude: 13.8493° N, longitude: 75.2997° E). The harvested leaves were hand-picked carefully to remove any diseased or damaged leaves and then washed thoroughly three times with distilled water to remove stuck dust, soil particles, and other surface stains. The washed leaves were subsequently air-dried in shade at room temperature for one week to avoid exposure to direct sunlight, which would cause degradation of bioactive compounds. After total drying, the leaves were well chopped and ground into a coarse powder form using a mechanical grinder. Powdered material was kept in airtight glass containers under cool and dry conditions until use. For the preparation of the aqueous extract, 10% (w/v) powdered betel leaf was dissolved in distilled water. The solution was heated slowly on a hot plate under constant stirring using a magnetic stirrer for about 30 minutes. Temperature was kept low to prevent heat-induced degradation of the bioactive compounds. On heating, the solution slowly shifted color from light yellow to dark brown, showing the release of phytochemicals into the aqueous medium. The mixture was then cooled naturally to room temperature after heating. The extract was filtered using Whatman No. 1 filter paper to eliminate particulate matter and get a clear solution. Filtered extract was taken in sterile tubes and kept at 4 °C in a refrigerator for future experimental purposes (Fig. 1a).

2.2 Preparation of zinc oxide nanoparticles *via* green synthesis

Piper betle leaf extract served as a stabilizer and reducing agent for the green synthesis of ZnO NPs. Initially, 0.2195 g of zinc acetate dihydrate [$Zn(CH_3COO)_2 \cdot 2H_2O$] (analytical grade, 99% purity) was accurately weighed and dissolved in 50 mL of distilled water to prepare a 0.02 M solution. Magnetic stirring was done for sterile dissolution and homogeneity of solutions. After 10 minutes of continuous stirring, an aqueous extract of *Piper betle* leaves was added dropwise to the stirred aqueous solution of zinc acetate. Stirring was continued to allow for interaction between the zinc ions and phytochemicals present in the plant extract, which act naturally as capping and stabilizing agents. This solution was made basic by the slow addition of 2.0 M sodium hydroxide solution to start the formation of ZnO NPs. The addition of NaOH increased the pH of the solution to nearly 12, and a severely pale whitish colloid suspension formed, indicating the nucleation of zinc hydroxide complexes, which would form ZnO NPs later on. The reaction mixture was stirred magnetically for 2 hours at room temperature for complete reduction and stabilization. At the end of the reaction time, the obtained suspension was centrifuged at 10 000 rpm for 15 minutes to isolate the synthesized NPs.[26,27] The formation of ZnO NPs using betel leaf extract as a reducing and stabilising agent (BZnO NPs) was indicated with the formation of a pale white precipitate. The precipitate was carefully decanted and purified by washing it several times with distilled water and then with ethanol to remove unreacted precursors, phytochemicals, and other impurities. The pure BZnO NPs were dried overnight in a vacuum oven at 60 °C, yielding a fine pale white powder that was collected and stored in airtight containers for characterisation and further use (Fig. 1a).

2.3 Degumming of *Bombyx mori* silk fibres

Raw silk fibres obtained from the *Bombyx mori* silkworm were sourced from the Ramanagara Cocoon Market, Karnataka, India (latitude: 12.715035° N, longitude: 77.281296° E). The fibres in their natural form have a protective proteinaceous coating called sericin, also known as silk gum, which needs to be removed by a process called degumming to yield pure fibroin for further use. The degumming was performed according to a conventional soap-alkali process.[28] A degumming bath containing a silk-to-solution ratio of 1 : 40 was prepared. Flakes of soap and sodium carbonate were added in concentrations of 7 g L^{-1} and 1 g L^{-1}, respectively. Gradually, the solution was heated until boiling point. Once the degumming bath attained the required temperature, raw silk fibres were slowly added to the solution and boiled for 60 minutes. This process effectively stripped off the sericin coating. After the boiling process, the silk was gently taken out and washed repeatedly with cold distilled water to remove any remaining soap, soda, and sericin residues. For effective removal of the degumming agents as well as all residual gum, the fibres were washed one more time using hot water for 15 minutes. After the rinsing treatment, the degummed silk fibres were air-dried under shade conditions at ambient room temperature to ensure avoidance of any photodegradation or yellowing. The degummed silk fibres produced were soft, lustrous, and lacked the outer sericin layer, so they were ready for further processing or characterization.[29]

2.4 Coating of BZnO NPs on silk fibres

For the functionalization of the silk fibers with BZnONPs, a dispersion of NPs was first prepared. To begin with, a 0.2% (w/

v) aqueous dispersion was obtained by dissolving 0.2 g of previously synthesized BZnONPs in 50 mL of ultrapure water. The dispersion was sonicated and magnetically stirred throughout to ensure stable and uniform distribution of the nanoparticles in the solution. In this process, sodium alginate was utilized as a biocompatible, eco-friendly binder which may promote the adhesion of BZnONPs onto the surface of silk fibre. Degummed silk fibres were immersed in a solution of sodium alginate to enhance the holding of the NP. As the next step, alginate-functionalized silk fibres were then immersed in the dispersion of NP. The coating process was conducted at a regulated temperature of 40 °C with gentle agitation to provide homogeneous suspension and enable interaction between the fibre surface and the distributed BZnONPs. The pH of the dispersion was also adjusted and maintained at 7.7, which was found to be optimal for the effective binding of BZnONPs on the silk substrate. The fibres were left under these conditions in the NP solution for one hour. Following incubation, the BZnONPs-coated silk fibres were removed from the dispersion, gently washed with distilled water to eliminate loosely bound nanoparticles or excess reagent, and air-dried at room temperature under shade to maintain their structural integrity and avoid photodegradation (Fig. 1b). The coated silk fibres were then stored in a clean, dry environment for characterization and subsequent analysis.[30]

2.5 Approaches for characterization

The optical properties of BZnONPs were examined by UV-Visible spectrophotometry to observe the bioreduction of zinc ions. A double-beam UV-Vis spectrophotometer (Shimadzu) was utilised to measure the absorption spectra of the reaction mixture in the range of 200–800 nm. Spectral measurements were performed at intervals to monitor the formation and stability of BZnONPs. FTIR spectra were collected in attenuated total reflectance (ATR) mode using a PerkinElmer Spectrum 3 Tri-Range FTIR spectrometer. This was performed to identify the functional groups in the betel leaf extract and their involvement in the reduction and stabilization of NPs and the effective coating over silk fiber. The spectra were taken in the wavelength range from 4000 to 400 cm^{-1} with a resolution of 4.0 cm^{-1}. Morphological features, surface topography, and structural properties of synthesised BZnONPs, uncoated silk fibers and BZnONP-coated silk fibers were analysed using SEM (Thermo Scientific Apreo 2S). The sample was analyzed at an accelerating voltage of 3 kV and under different magnifications. The hydrodynamic size distribution and surface charge were further determined by a Dynamic Light Scattering (DLS) analyzer (Zetasizer Nano ZS, Malvern, UK). Zeta potential analysis was performed at 25 °C to assess the colloidal stability of the produced nanoparticles. The zeta potential value, expressed in millivolts (mV), was employed to calculate the surface charge of the NPs and their electrostatic stability within the solution. Finally, X-ray diffraction (XRD) analysis was performed using a (Rigaku MiniFlex 600, Japan) to determine the crystalline structure and phase purity of the biogenically synthesised BZnONPs and silk fibers with and without coating.

2.6 Determination of mechanical strength of silk fibres

The mechanical performance of uncoated and BZnONPs-coated silk fibres was studied to determine the effects of thermal treatment and surface feature changes on durability and tensile strength behaviour. Pre- and post-autoclave sterilization measurements were considered for possible biomedical or industrial applications, where thermal stability and mechanical stability of coated silk are of utmost importance. Silk fibres approximately 12 cm long were selected for each of the tests and placed in the grips of the UTM (Universal Test Machine) (Instron 5943, Instron, USA). The fibres were positioned in the vertical plane so that during tensile testing, uniform stress would be applied along the axial direction. The tests were conducted under normal room ambient conditions. With the lower grip of the UTM set to move at a constant crosshead speed of 5 mm min^{-1}, increasing tensile load was applied to rupture the fibre sample. The machine records the maximum load (N) being carried by the fibre before rupture and measures breaking strength (MPa) which is a measure of the tensile strength of that material. Three repetitions of these tests were then carried out for reproducibility and statistical relevance. Average values and standard deviation were calculated and tabulated for comparison purposes between the coated and uncoated fibre samples and between the pre and post-autoclaving conditions.[31] This analysis enables us to assess the influence of NP coating and thermal sterilization on the structural integrity and functionality of silk fibres with special reference to their application in biomedical and textile technology.

2.7 Determination of antibacterial activity

The antibacterial efficacy of BZnONPs-coated silk fibres against the Gram-positive bacterial strain *Staphylococcus aureus* (MTCC 87, Chandigarh, India) was evaluated by the standard agar diffusion method. One loopful of one *S. aureus* colony was inoculated into 100 mL of pH 7.4 sterile Luria-Bertani (LB) broth and incubated at 37 °C on an orbital shaker with agitation at 180 rpm for 18–24 hours to obtain an active culture. Once the bacterial culture reached the lag phase, it was uniformly spread on the surface of sterile Mueller–Hinton Agar (MHA) plates using a sterile cotton swab to create an even lawn of bacteria. Pre-sterilised silk samples were aseptically cut into equal pieces and gently placed on the inoculated agar surface without overlap for uniform contact. A concentration of 10 μg mL^{-1} of ciprofloxacin was employed as a positive control to generate experimental proof and ensure the reliability of antimicrobial assay. The antibiotic was used in its free form, not incorporated inside the silk fibers. The main reason for using ciprofloxacin was not to compare its release profile with BZnONPs-coated silk fibres, but rather to use it as a reference standard for comparison of antibacterial activity. Uncoated silk fibers were used as a negative control to demonstrate the baseline behavior of the substrate. The plates were then incubated at 37 °C for 24 hours aerobically. After incubation time, the plates were imaged with digital images taken, and the antibacterial activity was quantified as the diameter of the transparent inhibition zones surrounding the silk samples (Fig. 1c). The zone of inhibition

represented the extent to which the bacterial growth was inhibited.[32] Bigger inhibition zones were associated with more active antibacterial activity. All experiments were repeated in triplicate to verify reproducibility, and mean values were computed for comparison.

2.8 Evaluation of biocompatibility

Biocompatibility testing of both uncoated silk fibres and BZnONPs-coated silk fibres was performed on normal red blood cells (RBCs), peripheral lymphocytes, and cell lines. A haemolysis assay was performed to investigate the impact on normal RBCs. Fresh sheep blood obtained from a local butcher was stabilised with EDTA. The blood was centrifuged at 700 g for 5 minutes to isolate the plasma and buffy coat. The rest of the RBC pellet was washed three to four times with phosphate-buffered saline (PBS) and diluted subsequently with PBS to prepare a volume of up to 25 mL. For the haemolytic test, fibre sample suspensions in PBS were blended with 0.2 mL of RBC suspension and incubated at various pH levels. Positive and negative controls were set up by adding 0.8 mL of 2% Triton X-100 and PBS, respectively, to 0.2 mL of RBC solution. Samples were then left to incubate for 2 hours at room temperature with frequent mixing every 30 minutes to prevent sedimentation. Mixtures were centrifuged at 700 g for 5 minutes, and 100 μL of supernatant was taken and transferred into a 96-well plate. The release of haemoglobin was then assayed at 570 nm with a microplate reader and percentage haemolysis was calculated to quantify membrane damage.[33,34]

To assess the impact of the fibres on the immune cells, peripheral lymphocytes were isolated from freshly collected blood. Blood was mixed with an equal volume of Ficoll-Paque™ Plus solution (GE Healthcare, Sweden), layering this mixture into a standard density centrifuge tube, and spinning the mixture at 3000 rpm for 20 minutes at 18 °C. The lymphocyte-rich fraction was carefully collected and washed twice with PBS by centrifugation at 2000 rpm for 10 minutes at 18 °C, then resuspended in RPMI-1640 medium supplemented with 10% fetal bovine serum. Cell concentration was determined using a hemacytometer and the viability was assessed using the trypan blue exclusion method. The lymphocytes were transferred to 96-well plates in a humidified 5% CO_2 atmosphere at 37 °C, to which phytohemagglutinin (PHA, 10 μg mL^{-1}) was added to stimulate lymphocyte proliferation. Following exposure of the fibre samples for varying time intervals, an assessment of their proliferation was done using an MTT assay. Briefly, 5×10^3 lymphocytes per well were seeded, and the fibers were introduced during the indicated periods. When the treatment was terminated, the medium was discarded, then added with 1 mg mL^{-1} MTT reagent was added, and incubated at 37 °C for 4 hours. The formazan crystals produced by viable cells were dissolved in DMSO, and using a microplate spectrophotometer, absorbance was recorded at 570 nm.[35]

The cytotoxicity tests of silk fibres were carried out using two cell lines, mouse embryonic fibroblasts (3T3-L1) and human cervical carcinoma (HeLa) cells. Both cell lines were obtained from the National Centre for Cell Science (NCCS), Pune, India, and were maintained in Dulbecco's Modified Eagle Medium (DMEM; Gibco, USA) with 10% heat-inactivated fetal bovine serum (FBS) and 1% antibiotic–antimycotic solution comprising 10 000 U per mL penicillin, 10 000 μg per mL streptomycin, and 25 μg per mL amphotericin B. The cells were maintained at 37 °C under a humidified atmosphere of 5% CO_2. Cells which were 80–85% confluently were subcultured using 0.25% trypsin–EDTA solution and the culture medium was replaced every 48 hours every time. Before the intended experiments, cell viability was determined using the trypan blue exclusion method. Cells greater than 95% viability were used for subsequent assays. The cytotoxicity of silk fibres was evaluated with an MTT assay as mentioned above, where each experiment was performed in triplicate with untreated cells serving the role of negative controls (Fig. 1c).

2.9 Statistical analysis

The data were expressed as the mean ± standard deviation (SD) of the three replicates and analyzed using Graph Pad PRISM software version 5.0 (San Diego, USA). One-way analysis of variance was used for the repeated measurements, and the differences were considered to be statistically significant if $p < 0.05$.

3. Results and discussion

3.1 Fabrication of biogenic nanoparticles

The green synthesis of BZnONPs by *Piper betle* leaf extract was an effective, eco-friendly, and sustainable method of NP fabrication. This approach not only prevents the use of toxic chemical reagents and extreme physical conditions but also takes advantage of the innate biochemical variability present in betel leaves. Aqueous leaf extract of *Piper betle* has a diverse stock of bioactive phytochemicals like flavonoids, alkaloids, phenolics, tannins, and terpenoids.[18] These compounds served a dual purpose in the synthesis process, performing the role of reducing agents that enable the bioreduction of zinc ions to ZnO as well as that of stabilizing or capping agents inhibiting agglomeration and inducing the stability of the resulting NPs.[24] In the course of the reaction, the rapid colour transformation from pale yellow to whitish suspension was noticed, demonstrating the initiation of the formation of BZnONPs (Fig. 2a). This color change is owing to surface plasmon resonance (SPR), a phenomenon usually linked with the presence of metal or metal oxide NPs. SPR results from the total vibration of conduction electrons on arrival of light, which depends on size, shape, and medium. The color change was an initial verification of NP synthesis and was in line with other reports of biosynthesis.[36] Our results confirm that betel leaf extract can successfully mediate the synthesis of stable, homogeneous nanoparticles by using a straightforward one-pot procedure without the use of toxic solvents or drastic reaction conditions. Other physicochemical properties will also be vital to investigate the properties and biological applications of BZnONPs.

3.2 Characterisation of BZnONPs

Characterisation of BZnONPs was performed using various analytical methods to validate their structural and functional

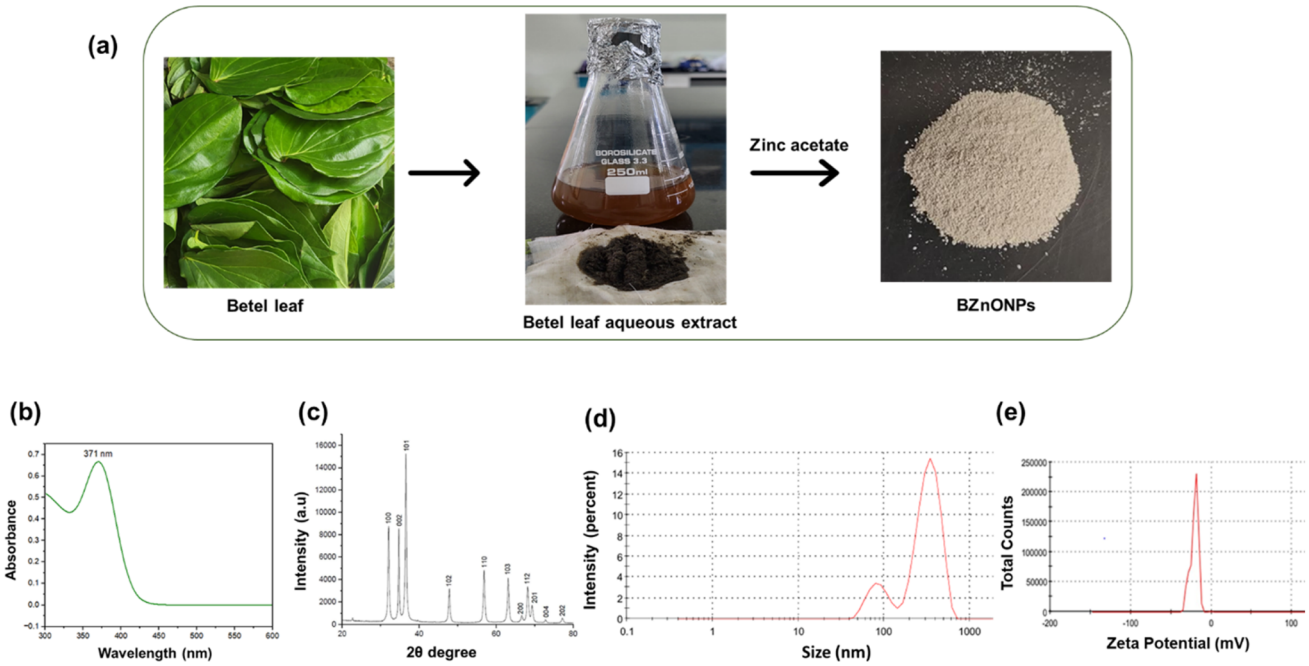

Fig. 2 Biogenic fabrication and characterization of zinc oxide nanoparticles. (a) Schematic representation of the synthesis of zinc oxide nanoparticles using betel leaf extract as a reducing and stabilizing agent (BZnONPs). (b) UV-Visible absorption spectrum of BZnONPs showing a characteristic surface plasmon resonance peak, confirming nanoparticle formation. (c) X-ray diffraction pattern indicating crystalline nature and phase purity. (d) Zeta potential and (e) size analysis of BZnONPs.

characteristics. UV-Vis spectrophotometric analysis validated the occurrence of ZnONPs with a clear SPR peak at 371 nm (Fig. 2b). The peak is consistent with reported values for ZnONPs prepared from materials of biogenic origin. The UV-Vis spectrum of BZnONPs revealed monodisperse, isotropic NPs with sharp optical features.[37] The XRD pattern from the synthesised BZnONPs confirmed its crystalline nature. The peaks of diffractions observed at 2θ values of 32.09°, 36.56°, 47.84°, 56.89°, 63.14°, 66.7°, 68.22°, 69.36°, and 77.26° corresponded well with the standard hexagonal wurtzite structure of ZnO, indexed to (100), (002), (101), (102), (110), (103), (112), and (202) crystal planes, respectively (Fig. 2c and Table 1). All the findings are well in agreement with the Joint Committee on Powder Diffraction Standards (JCPDS) card no. 36-1451, confirmed successful formation of ZnONPs, but the little few unindexed peaks could be attributed to residual organic invoked from *Piper betle* leaf extracts and hence suggested impurity due to the green synthesis method (Table S1).[38] Average crystallite size analyses using the Debye–Scherrer formula revealed that the BZnONPs had approximately 15.65 nm dimensions, which seem to be on a nanoscale with good crystallinity. The results certified that the phytochemical-mediated green synthesis route was not only efficient in NP formation but yielded BZnONPs with desirable structural properties.[14]

DLS measurement was conducted to determine the hydrodynamic size distribution and colloidal stability of biologically synthesised BZnONPs. The results showed that the hydrodynamic mean diameter of the BZnONPs was greater than 200 nm under optimised synthesis conditions (Fig. 2d). This size includes not only the NP core but also the layer of solvent and phytochemical capping agents on top of it, which usually enhances the measured size in DLS measurement. The relatively uniform particle size distribution proved successful synthesis and stabilisation by bioactive compounds in the plant extract. Moreover, the zeta potential of the BZnONPs was found to be −20.8 mV (Fig. 2e), proving moderate to high colloidal stability in water suspension. This negative surface charge is indicative of the presence of electronegative functional groups, which are likely to be phenolic or carboxyl groups of phytochemicals of the *Piper betle* extract as natural capping and stabilising entities. These phytochemicals on the surface avoid NP

Table 1 XRD data of BZnONPs showing 2θ values (°), absolute intensities (a.u.), and relative intensities (%). The relative intensity is calculated to the most intense diffraction peak, indicating the degree of crystallinity and preferred orientation of the synthesised BZnONPs

BZnONP		
2θ (°)	Absolute intensity (a.u.)	Relative intensity (%)
32.09055	9000	56.30%
36.56776	16 000	100%
47.84721	2500	15.60%
56.89522	4000	25.00%
63.14653	3600	22.50%
66.76783	3000	18.80%
69.34768	1900	11.90%
72.83301	1600	10.00%
74.5057	1500	9.40%

agglomeration by providing an effective electrostatic repulsion between individual particles. Zeta potential measurement is crucial in assessing NP stability because it reflects the magnitude of surface charge and repulsion between similarly charged particles suspended in the medium. A zeta potential of over ±20 mV is always considered adequate to ensure colloidal stability in different physiological conditions.[25,39] For BZnONPs, the formation of an electrical double layer around the particles results in repulsion, thus increasing the stability over time. This finding supports the efficacy of green synthesis in the creation of stable suspensions of particles suitable for biomedical and environmental applications.

3.3 Preparation of BZnONP-coated silk fibres

Raw *Bombyx mori* silk fibres were treated with a routine degumming procedure, boiling in a mild alkaline solution to remove the sericin layer, a hydrophilic glycoprotein natural coating of silk fibres. Visual and tactile examination of the fibres after degumming showed a clear change. The fibres had a glossy, smooth surface and enhanced softness, confirming successful removal of sericin (Fig. 3a). This was complemented by the lack of residual coating observed using light microscopy and a considerable decrease in mass that was consistent with the anticipated content of sericin. Removal of sericin is also important since it not only improves the purity and biocompatibility of the silk fibroin but also reveals active functional groups to be used for further surface modification.[29] This is very important for making use in biomedical applications such as wound dressings. After degumming, the purified silk fibroin fibres were functionalized with BZnONPs. Sodium alginate was utilised as a bio-adhesive medium owing to its good film-forming property, biodegradability, and compatibility with inorganic NPs as well as natural fibres. Alginate usage ensured a homogeneous and stable BZnONP coating on the silk surface. Degumming produced clean, fibroin-enriched silk fibres, which are amenable to surface functionalization using appropriate chemical entities.[30] The BZnONPs were successfully immobilised on the silk surface through the use of sodium alginate, resulting in the formation of a composite material for different applications after suitable characterisation.

3.4 Functional characterisation of BZnONP-coated silk fibres

FTIR spectroscopy is an analytical technique used for the identification of functional groups and molecular interactions in organic and inorganic compounds. FTIR spectroscopy was a core instrument in this work to evaluate each step of the fabrication process, ranging from synthesising BZnONPs to coating them onto degummed *Bombyx mori* silk fibres. This research permitted confirmation of the presence of phytochemicals of plant origin, successful synthesis of NPs and incorporation of BZnONPs into the silk matrix. FTIR spectrum of the betel leaf extract revealed characteristic broad absorption bands at 3300–3400 cm^{-1} corresponding to O–H stretching

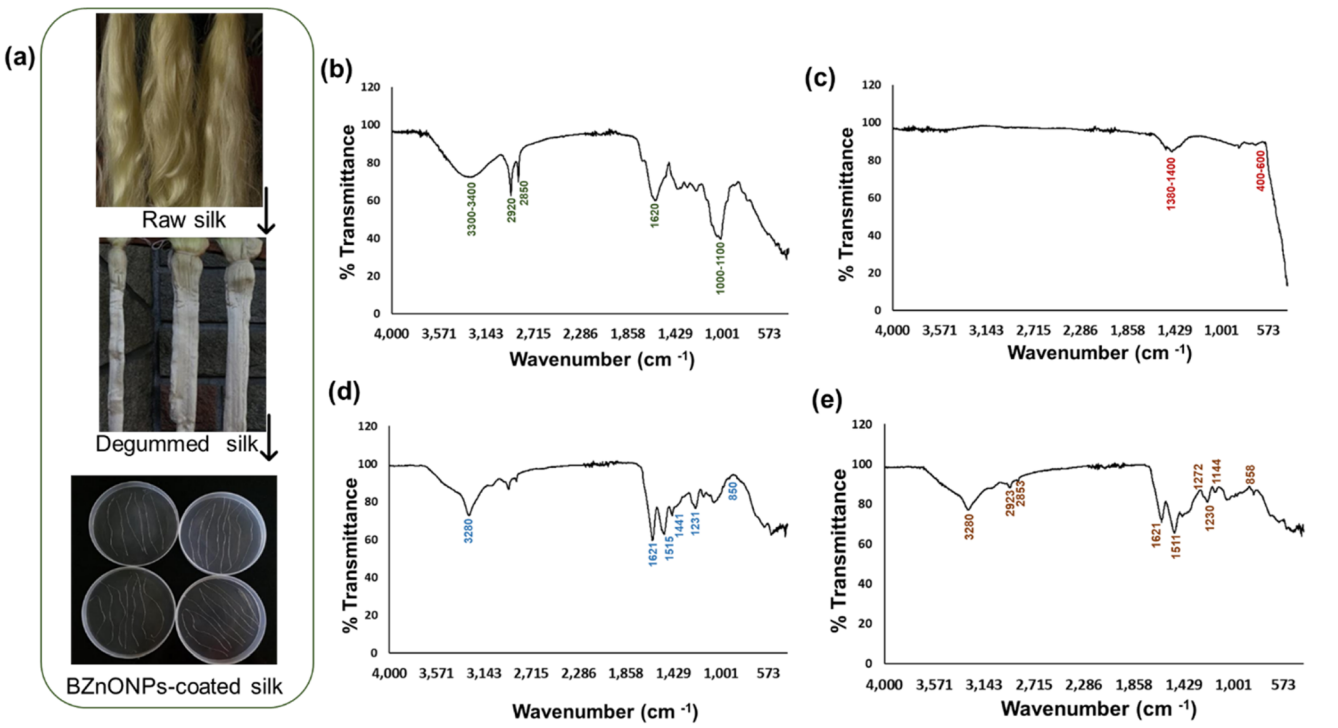

Fig. 3 Preparation and FTIR-based characterization of BZnONP-coated silk fibres. (a) Schematic representation of the fabrication process, including degumming of *Bombyx mori* silk fibres to remove the sericin layer and subsequent surface functionalization with BZnONPs. FTIR spectral analysis showing the characteristic functional groups in (b) betel leaf extract, (c) biosynthesized BZnONPs, (d) degummed silk fibres, and (e) BZnONP-coated silk fibres, confirming successful synthesis, surface interactions, and coating efficiency.

vibrations by alcoholic and phenolic groups, mostly present in the bioactive compounds such as eugenol, chavicol, and other phenylpropanoids found in the betel leaf (Fig. 3b). Additionally, bands at 2920 cm^{-1} and 2850 cm^{-1} correspond to symmetric and asymmetric C–H stretching vibrations, respectively, supporting the presence of aliphatic chains of plant metabolites. A sharp peak at 1620 cm^{-1} was attributed to C=C stretching vibrations, thereby establishing the existence of aromatic rings in the extract. The C–O stretching vibrations in the 1000–1100 cm^{-1} region point toward the existence of alcohols, esters, or polysaccharides commonly found in plant extracts.[40] In BZnONPs, Zn–O stretching vibrations occurred in the fingerprint region of 400–600 cm^{-1}, thus confirming successful ZnONP formation (Fig. 3c). Other minor peaks near 1380–1400 cm^{-1} were attributed to C–H bending or NO_3^- vibrations, which may be indicative of residual traces of precursor materials or side products during the green synthesis process.[17]

FTIR also characterised degummed silk fibroin to provide a structural reference. The amide A band, due to N–H stretching, appeared at 3280 cm^{-1}, a characteristic feature of proteinaceous materials. The amide I band at about 1620 cm^{-1} (peptide bond C=O stretching) and amide II band at 1510 cm^{-1} (N–H bending and C–N stretching) attested to the presence of the characteristic β-sheet crystalline structure in silk fibroin. The amide III band at 1230 cm^{-1} also supported the protein backbone by way of C–N stretching and N–H bending vibrations.[41] Other low-intensity peaks consisted of a band around 850 cm^{-1}, attributed to out-of-plane C–H bending, generally seen with aromatic amino acid residues or remaining structural motifs in fibroin (Fig. 3d). After functionalizing degummed silk with BZnONPs, FTIR analysis displayed merged spectral signals, reflecting the successful coating and interaction between silk fibroin, BZnONPs, and bioactive phytochemicals derived from the betel leaf extract. Importantly, the existence of bands at 2850 and 2920 cm^{-1} again confirmed the occurrence of phytochemical residues, indicating that capping agents in the plant extract remained attached to the nanoparticles after coating. The Zn–O bond peak in the 400–600 cm^{-1} range was maintained, ensuring that the ZnO NPs were properly integrated into the silk fibres (Fig. 3e). BZnONPs exhibit only weak spectral features in the infrared region and are present as a surface coating. Consequently, their spectral contribution is minimal and can be easily masked by the dominant absorption bands of the silk matrix. However, there was a significant difference in the spectral signature between silk fibre and BZnONP-coated silk when the interpretation is focused between wave numbers 16000 and 400 cm^{-1} (Fig. S1). Notably, the amide I (1620 cm^{-1}), amide II (1510 cm^{-1}), and amide III (1230 cm^{-1}) bands were maintained in the coated fibres, indicating that the secondary structure of the protein in silk fibroin. Nonetheless, minimal changes in the N–H stretching peak at ~3280 cm^{-1} were noted, indicating intermolecular interactions or hydrogen bonding between bioactive compounds, protein backbone, and ZnO surface. In addition, the 1100 cm^{-1} band due to C–O–C and C–N stretching was stronger in the coated samples, reflecting good capping and stabilisation by the phytochemicals, which would have improved the binding affinity of the BZnONPs with the silk matrix.[29,30,42] In the case of Fig. 3d and e, the spectra appear more or less identical due to the strong absorption bands of silk and the poor infrared signature of the nanoparticles, as had been noted for the spectrum of pure BZnONPs. Since the BZnONPs are surface coatings on the silk fibers, from the composite spectrum view, their contribution remains too low and could be masked by the peak of pure silk. However, going lower in the wavenumber scale, to 600–400 cm^{-1}, faint yet distinct features linked to Zn–O vibrations could be detected, thereby confirming the actual presence of BZnONPs.

3.5 Structural characterisation of BZnONP-coated silk fibres

The biosynthesised BZnONPs were characterised using SEM in terms of their surface morphology and deposition on degummed silk fibres. SEM images of BZnONPs show quasi-spherical-shaped NPs, with little agglomeration, which is typical of green-synthesised metal oxides due to phytochemical capping agents (Fig. 4a). Surface texture of degummed *Bombyx mori* silk fibers indicated sleek, homogeneous, and cylindrical shapes of fibers along with a spotless surface, indicating successful removal of the sericin coat during the degumming process. Free of surface irregularities, further testified the purity of the exposed fibroin core (Fig. 4b). After coating, the BZnONP-functionalized silk fibres had a complete change in surface texture when viewed under the SEM micrographs, contrary to that of the uncoated fibres. The flawless surface of degummed silk was replaced by a visibly rougher nature, which indicates successful adsorption of the BZnONPs. Which appeared as discrete particulate layers or agglomerations stuck onto the fibroin matrix (Fig. 4c). EDS was used to investigate the elemental composition of BZnONPs and the coated degummed silk fibres. BZnONPs showed the presence of carbon from active phytochemicals from the leaf extract of the betel used during the green synthesis (Fig. 4d). EDS analysis revealed zinc and oxygen elements for BZnONP-coated silk fibers, confirming successful coating of BZnONPs on the fiber surface. Additionally, strong signals were registered for carbon and nitrogen. The nitrogen signal is coming from the proteinaceous nature of the silk fibroin, while the source of carbon is both from the silk matrix and capping agents derived from plants (Fig. 4e). EDS analysis confirmed the presence and surface distribution of key elements—zinc (Zn), oxygen (O), and carbon (C)—on the coated samples. Notably, the detectable Zn signal on the BZnONPs-coated silk, absent in the uncoated counterpart, supports the successful and uniform deposition of ZnO nanoparticles onto the silk matrix (Table S2). The presence of all four elements in the coated fibers shows successful binding of the BZnONPs onto the silk surface.[42,43]

3.6 Mechanical strength analysis of coated and uncoated silk fibres

Mechanical testing was under the peak load of 2.3 kg to compare uncoated and BZnONP-coated *Bombyx mori* silk fibres (Table 2). The BZnONPs-coated unsterilized silk fibres exhibited considerably higher tensile strength of around 2.2 N m^{-2} compared with uncoated, unsterilized control fibres exhibiting minimum tensile strength, determined to be approximately

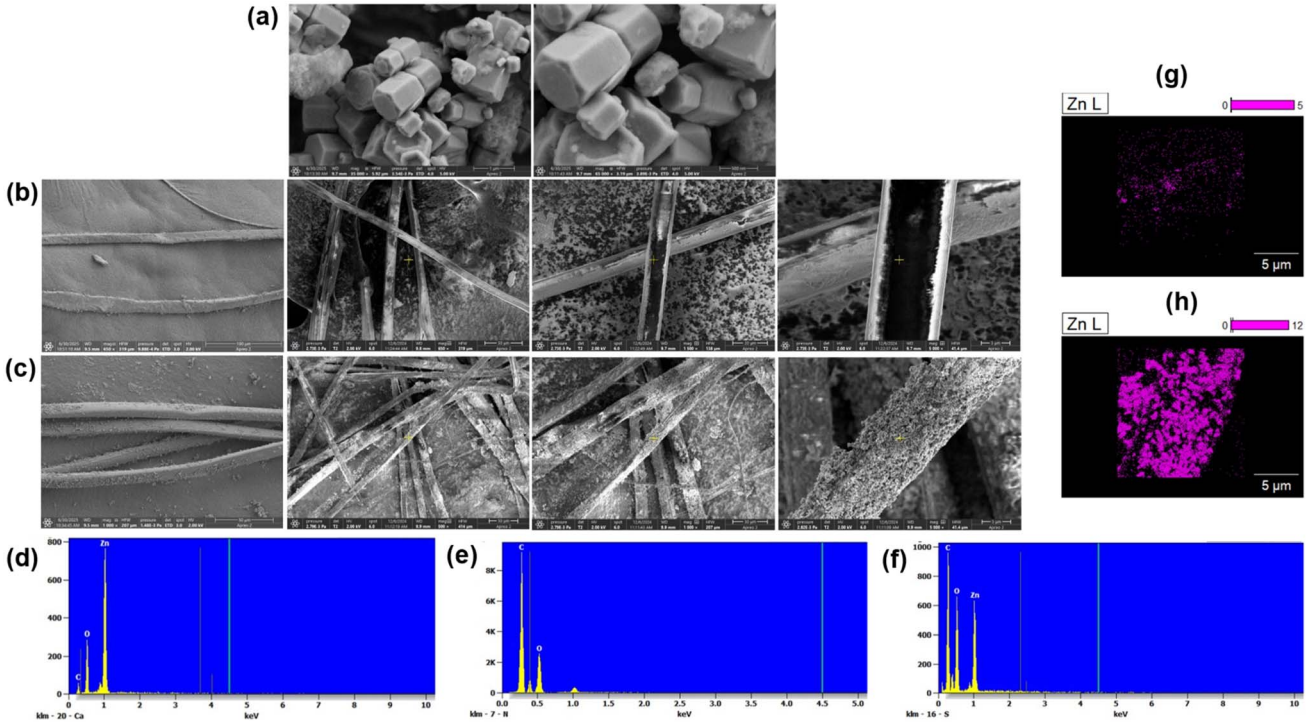

Fig. 4 SEM images captured at various magnifications illustrating the surface morphology of (a) BZnONPs, (b) uncoated silk fibers, and (c) silk fibers coated with BZnONPs. The micrographs highlight the distinct structural features and distribution patterns of the nanoparticles on the silk surface. EDS spectra presented in (d) confirm the elemental composition of the synthesized BZnONPs. At the same time, (e) shows the EDS profile of the uncoated silk and (f) denotes BZnONP-coated silk, indicating successful deposition of nanoparticles onto the silk substrate. Elemental mapping of Zn on (g) uncoated and (h) BZnONP-coated silk fibres.

0.83 N m^{-2}. This tremendous improvement in mechanical strength suggests that surface functionalization by BZnONPs serves a protective function for the silk structure. The enhancement of tensile strength can be attributed to two principal factors. Firstly, the degumming process, which removes the sericin coating, exposes the fibroin core and facilitates enhanced NP adhesion and uniform coating. This also facilitates potential cross-linking interaction between the phytochemical-capped BZnONPs and the fibroin, thereby enhancing the mechanical strength of the fibre. Second, the addition of BZnONPs triggers stiffening in the fibre matrix by reinforcing the protein scaffold and removing surface defects that could otherwise serve as sites of mechanical failure.[44] However, autoclaving has had a detrimental effect on the mechanical properties of both coated and uncoated fibres. Therefore, it is apparent that sterilisation has brought significant loss in tensile strength, as being autoclaved under high-temperature and high-pressure conditions rearranges the molecular structure and partially degrades the protein structure. An increase in tensile strength is attributable to the NP adhesion, a pendant cross-linking with the fibroin core, and the reinforcement of the protein scaffold. Though autoclaving caused a general degradation in tensile strength through thinning and structural degradation, compared to uncoated fibres, the BZnONP-coated fibres retained relatively higher strength probably due to the coating bearing some protective effects. Nevertheless, BZnONP-coated in comparison to uncoated fibers, demonstrated relatively higher tensile strength following sterilisation, indicating that this NP coating provides some thermal degradation protection, probably blocking heat and

Table 2 Tensile strength of coated and uncoated silk. Data are represented as mean ± standard deviation ($n = 3$). An F-test (one-way ANOVA) was conducted to compare the means between groups. Coating with BZnONPs significantly increased the mechanical strength of silk fibres both before and after autoclaving, as shown by higher means and extremely low p-values

Test groups	Peak load at break (kg) (before autoclave)	Peak load at break (kg) (after autoclave)	Ultimate tensile strength (N m^{-2}) (before autoclave)	Ultimate tensile strength (N m^{-2}) (after autoclave)
Uncoated silk fibres	0.85 ± 0.04	0.32 ± 0.03	0.83 ± 0.05	0.30 ± 0.04
BZnONP-coated silk fibres	2.30 ± 0.15	1.80 ± 0.10	2.25 ± 0.10	1.20 ± 0.08
F-Value	261.72	602.86	483.94	303.75
Significance	0.0000854	0.0000163	0.0000253	0.0000636

moisture-mediated denaturation from the environment.[31] The obtained *p*-values ($p < 0.001$) indicate statistically significant improvements in tensile strength of BZnONP-coated silk fibres compared to uncoated controls, both before and after autoclaving.

3.7 Antibacterial activity of BZnONP-coated silk fibres

The antibacterial effectiveness of BZnONP-coated silk fibers was investigated against *Staphylococcus aureus* (*S. aureus*), a Gram-positive bacterium that frequently inhabits the surfaces of biomaterials, particularly the very hygroscopic ones, such as silk. Clear inhibition zones were observed around the BZnONP-coated silk fibers (Fig. 5a), after incubation for 24 hours at room temperature, while the uncoated fibers showed no inhibition zones. The action of coated silk against *S. aureus* may be attributed to several interrelated mechanisms. It is to be noted that ciprofloxacin was used merely as a free drug positive control to check sensitivity and to observe antimicrobial responsiveness in the assay. The antibacterial effect seen with the BZnONP-coated silk fibers, which was not present in the corresponding uncoated controls, demonstrates the nanomaterial coating's intrinsic antimicrobial property. Future investigations will focus on the detailed investigation of release profiles and their possible connection with a prolonged antimicrobial effect when antibiotics or other bioactive molecules are embedded within the silk matrix. ZnONPs interfere with bacterial viability *via* multiple mechanisms, including direct contact with the bacterial cell wall and the production of reactive oxygen species. Zn^{2+} are membrane-damaging and induces oxidative stress, resulting in cell death. The effects are much more significant against Gram-positive *S. aureus*, with poor defence mechanisms against NP-mediated oxidative and ionic stress, because its relatively thicker peptidoglycan layer cannot provide sufficient protection.[32,45] The fibres of silk are inherently hydrophilic and porously structured, and thus highly susceptible to microbial attachment.

The reference strain of *S. aureus* MTCC 87 was used in this work because it is well-characterized and reproducible in antimicrobial testing. It is not antibiotic-resistant but effectively demonstrates the intrinsic antibacterial activity of the BZnONP-coated silk fibers, thereby supported by the observed activity. Since silk is capable of moisture retention and nutrient absorption, it can also promote the growth of bacteria; thus, BZnONP coating can inhibit the adhesion and disrupt the proliferation of bacteria. Since *S. aureus* is a principal agent for skin and surgical infections, its test on drug-resistant strains such as MRSA will further validate its clinical relevance.[9,46] The antibacterial activity displayed by BZnONP-coated silk fibers thus also suggests their vast potential as medical sutures, wound dressings, and tissue scaffolds, where BZnONPs are beneficial in interfacial strength, which is critical in the biomedical field involving silk-based biomaterials.

3.8 Biocompatibility evaluation of BZnONP-coated silk fibres

The as-prepared BZnONP-coated silk fibres had satisfactory physicochemical characteristics and higher antibacterial activity. However, the biomedicinal applications of the material are limited unless the activity toward blood cell counterparts and normal cells is analyzed.[13] To this end, the impact of coated and uncoated silk fibres was initially analyzed on RBCs through hemolysis assay. BZnONP-coated silk fibers and the bare silk showed a haemolysis percentage significantly below the acceptable limit in all the pHs attempted, indicating excellent

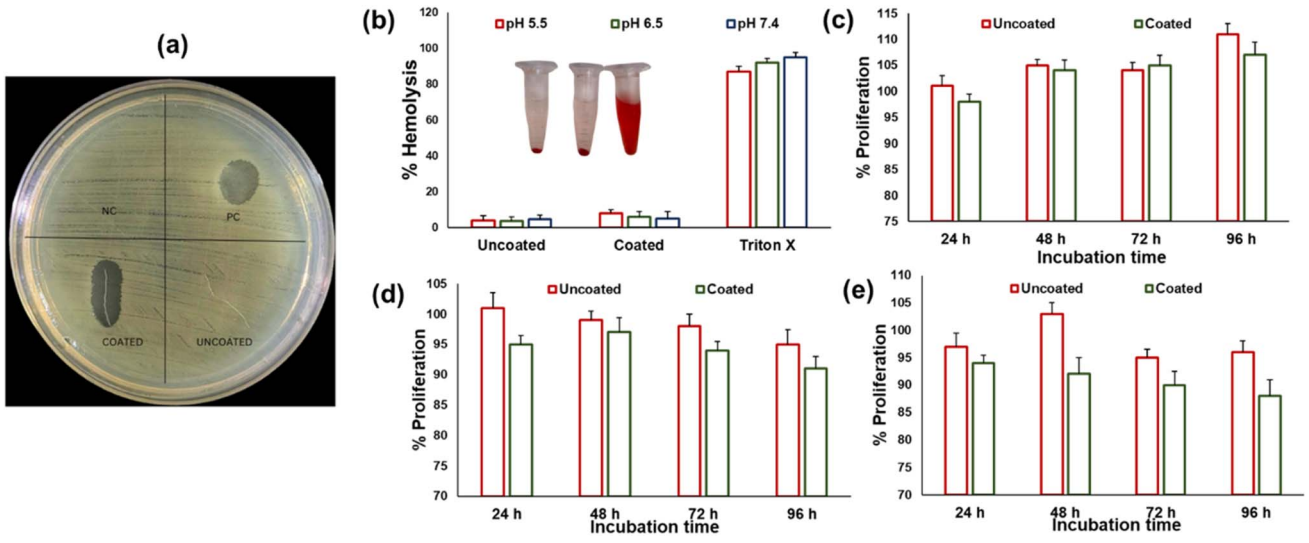

Fig. 5 Evaluation of the multifunctional performance of uncoated and BZnONP-coated silk fibres. (a) Antimicrobial activity assay against *Staphylococcus aureus*, indicating enhanced antibacterial properties upon nanoparticle coating. Biocompatibility assessments using various biological models. (b) Hemolysis assay with isolated peripheral red blood cells, (c) viability assay on isolated human lymphocytes, (d) cytotoxicity assay using a mouse fibroblast cell line and (e) human cervical carcinoma (HeLa) cell line. All results are presented as mean ± standard deviation (SD), based on experiments conducted in triplicate.

hemocompatibility (Fig. 5b). This low level of RBC lysis indicates that the coated fibers are unlikely to induce severe membrane damage or oxidative stress when they come into contact with blood. The hemolysis test is a critical test for any biomaterial that has to be used for biomedical applications that involve direct or indirect contact with blood. Low hemolysis rate indicates good hemocompatibility, and the material can safely be utilised as a wound dressing, suture, implant, or drug delivery system.[47] The immunocompatibility of the uncoated and BZnONP-coated silk fibres was examined by a lymphocyte proliferation assay with different incubation times (24 h, 48 h, 72 h, and 96 h). The uncoated silk fibres exhibited a moderate, time-dependent increase in lymphocyte proliferation, which suggested that native silk fibroin might weakly stimulate immune cells due to the inherent proteinaceous nature of the material or residual traces of sericin. Interestingly, the BZnONP-coated silk fibres were not cytotoxic to lymphocytes at any of the tested time points, indicating their biocompatibility. Also, a slight increase in lymphocyte proliferation was observed at 96 hours with the coated fibres, which may be attributed to the presence of bioactive phytochemicals in the betel leaf extract used in the synthesis of BZnONPs (Fig. 5c). The results confirm that BZnONP-coated silk fibres not only lack any form of toxicity towards immune cells but also can stimulate positive immune interactions, making them among the candidate materials for biomedical applications such as sutures, wound dressings, or scaffolds in tissue engineering.[19,35,48]

To assess the cytotoxicity of coated and uncoated silk-based biomaterials, *in vitro* cytotoxicity assays were carried out using two distinct cell lines. The murine fibroblast cell line (3T3-L1), which represents normal connective tissue cells, while the human cervical carcinoma cell line, HeLa, represents cancerous cells. Results showed that both uncoated and BZnONP-coated silk fibres were nontoxic to the 3T3-L1 cells at all time-periods tested, as evident from the sustained cell viability and proliferation (Fig. 5d). This supports the conclusion that silk fibres possess excellent cytocompatibility for biomedical applications such as tissue engineering and wound healing, which are based on interaction with normal fibroblastic cells. Interestingly, although HeLa cells maintained their viability at the earliest time intervals, BZnONP-coated silk fibres caused a pronounced drop in cell proliferation at 96 h. This suggests a time-limited cytotoxicity possibly resulting from the combined interaction of BZnONP and bioactive substances from the betel leaf extract with either the membrane or cytoplasm of cancer cells (Fig. 5e). Such bioactivity exemplifies the potential of these materials for applications in both regenerative medicine and cancer-inhibiting biomaterial platforms.[13,49] The slight toxicity of BZnONP-coated silk fibres toward cancer cells, although very minimal (percentage proliferation >85) suggests that the NPs may induce cell death through multiple mechanisms. ZnONPs have been reported to induce different cellular responses at varying concentrations, particle sizes and surface chemistry. One of the best-studied mechanisms is the production of reactive oxygen species, causing oxidative stress, mitochondrial impairment, and DNA damage, culminating in either apoptosis or necrosis.[50] NPs can affect cell membrane integrity, cause lipid peroxidation, and alter cellular signalling cascades important to sustaining cancer cell life.[51] Research has indicated that ZnONPs can induce lysosomal destabilisation and subsequent autophagy-associated cell death or apoptosis *via* caspase activation.[52] Because of their higher metabolic rates and redox imbalance, cancer cells are predisposed to such oxidative and intracellular stress relative to normal cells, which might contribute to the selectivity in cytotoxicity observed. The silk fibers were not cytotoxic to blood components, and only slightly toxic to healthy cells, suggesting that they are safe for possible use in biomedicine. Collectively, these results agree with previous reports demonstrating that ZnONPs can activate several pathways of cell death based upon cellular context and NP properties.[53]

Materials with more than 80% cell viability are rated as non-toxic according to common biocompatibility standards. Consequently, BZnONP-coated silk fibers are biocompatible and viable for biomedical applications. Their surface is conducive to cell adhesion and metabolic activity, and therefore potential for tissue engineering and wound healing. They exhibit low toxicity to normal cells and mild cytotoxicity towards cancer cells. Uncoated silk fibres occasionally enhanced cell growth beyond control levels, possibly as a result of the natural biocompatibility of silk and the mild stimulation of immunity, particularly in lymphocytes. PHA stimulation augmented this, raising metabolic activity. BZnONP coatings, on the other hand, dampened this response, possibly as a result of ZnO-mediated oxidative stress inhibiting cell viability.

4. Conclusion

This work deciphers the green synthesis of zinc oxide nanoparticles by *Piper betle* leaf extract and their effective loading onto degummed *Bombyx mori* silk fibers. The silk fibers coated with BZnONPs display an impressive boost in mechanical strength over uncoated controls alongside appreciable antibacterial activity against *S. aureus*. Of key significance is that these functionalized fibers prove to be high in hemocompatibility and immune-compatibility. This dual applicability, biocompatibility with healthy tissue, and antibacterial features, place BZnONP-coated silk fibers as multifunctional biomaterials with great prospects in wound healing, tissue engineering, and even cancer treatment. The green synthesis method further enhances the environmentally friendly aspect of this novel biomaterial, providing a more sustainable option compared to traditional methods in biomedical material engineering.

Conflicts of interest

There are no conflicts to declare.

Data availability

Supplementary information: The data supporting this article have been included as part of the SI. Any additional data can be provided upon request. See DOI: **https://doi.org/10.1039/d5ra03600c**.

Acknowledgements

The authors thank CHRIST University for the research facilities.

References

1 R. A. H. W. Chua, S. K. Lim, C. F. Chee, S. P. Chin, L. V. Kiew, K. S. Sim and S. T. Tay, Surgical site infection and development of antimicrobial sutures: a review, *Eur. Rev. Med. Pharmacol. Sci.*, 2022, **26**(3), 828–845, DOI: **10.26355/eurrev_202202_27991**.

2 J. L. Seidelman, C. R. Mantyh and D. J. Anderson, Surgical Site Infection Prevention: A Review, *JAMA*, 2023, **329**(3), 244–252, DOI: **10.1001/jama.2022.24075**.

3 A. Nespoli, S. Geroulanos, A. Nardone, S. Coppola and L. Nespoli, The history of surgical infections, *Surg. Infect.*, 2011, **12**(1), 3–13, DOI: **10.1089/sur.2010.106**.

4 K. M. Mueck and L. S. Kao, Patients at High-Risk for Surgical Site Infection, *Surg. Infect.*, 2017, **18**(4), 440–446, DOI: **10.1089/sur.2017.058**.

5 Y. Yang, Z. Zhou, R. Ma, J. Ren and X. Wu, Antimicrobial-coated sutures versus non-coated sutures in reducing surgical site infection: an updated systematic review and meta-analysis, *J. Hosp. Infect.*, 2024, **150**, 40–50, DOI: **10.1016/j.jhin.2024.04.027**.

6 N. Minoura, M. Tsukada and M. Nagura, Physico-chemical properties of silk fibroin membrane as a biomaterial, *Biomaterials*, 1990, **11**(6), 430–434, DOI: **10.1016/0142-9612(90)90100-5**.

7 T. Deptuch and H. Dams-Kozlowska, Silk Materials Functionalized via Genetic Engineering for Biomedical Applications, *Materials*, 2017, **10**(12), 1417, DOI: **10.3390/ma10121417**.

8 A. Scarano, F. Inchingolo, L. Leo, C. Buggea, A. Crisante, A. Greco Lucchina and G. Scogna, Bacterial adherence to silk and expanded polytatrafluorethilene sutures: an in vivo human study, *J. Biol. Regul. Homeostatic Agents*, 2021, **35**(2), 205–210, DOI: **10.23812/21-2supp1-21**.

9 T. Baygar, N. Sarac, A. Ugur and I. R. Karaca, Antimicrobial characteristics and biocompatibility of the surgical sutures coated with biosynthesized silver nanoparticles, *Bioorg. Chem.*, 2019, **86**, 254–258, DOI: **10.1016/j.bioorg.2018.12.034**.

10 Z. Dong, Q. Xia and P. Zhao, Antimicrobial components in the cocoon silk of silkworm, Bombyx mori, *Int. J. Biol. Macromol.*, 2023, **224**, 68–78, DOI: **10.1016/j.ijbiomac.2022.10.103**.

11 P. Yuan, X. Ding, Y. Y. Yang and Q. H. Xu, Metal Nanoparticles for Diagnosis and Therapy of Bacterial Infection, *Adv. Healthcare Mater.*, 2018, **7**(13), e1701392, DOI: **10.1002/adhm.201701392**.

12 S. Gharpure and B. Ankamwar, Synthesis and Antimicrobial Properties of Zinc Oxide Nanoparticles, *J. Nanosci. Nanotechnol.*, 2020, **20**(10), 5977–5996, DOI: **10.1166/jnn.2020.18707**.

13 M. M. Joseph, J. B. Nair, R. N. Adukkadan, N. Hari, R. K. Pillai, A. J. Nair, K. K. Maiti and T. S. Therakathinal, Exploration of Biogenic Nano-chemobiotics Fabricated by Silver Nanoparticle and Galactoxyloglucan with an Efficient Biodistribution in Solid Tumor Investigated by SERS Fingerprinting, *ACS Appl. Mater. Interfaces*, 2017, **9**(23), 19578–19590, DOI: **10.1021/acsami.7b03191**.

14 M. Irfan, H. Munir and H. Ismail, Characterization and fabrication of zinc oxide nanoparticles by gum Acacia modesta through green chemistry and impregnation on surgical sutures to boost up the wound healing process, *Int. J. Biol. Macromol.*, 2022, **204**, 466–475, DOI: **10.1016/j.ijbiomac.2022.02.043**.

15 G. Karunakaran, K. G. Sudha, S. Ali and E. B. Cho, Biosynthesis of Nanoparticles from Various Biological Sources and Its Biomedical Applications, *Molecules*, 2023, **28**(11), 4527, DOI: **10.3390/molecules28114527**.

16 H. Agarwal, S. Menon, S. Venkat Kumar and S. Rajeshkumar, Mechanistic study on antibacterial action of zinc oxide nanoparticles synthesized using green route, *Chem.-Biol. Interact.*, 2018, **286**, 60–70, DOI: **10.1016/j.cbi.2018.03.008**.

17 J. Sachin, N. Singh, R. Singh, K. Shah and B. K. Pramanik, Green synthesis of zinc oxide nanoparticles using lychee peel and its application in anti-bacterial properties and CR dye removal from wastewater, *Chemosphere*, 2023, **327**, 138497, DOI: **10.1016/j.chemosphere.2023.138497**.

18 M. Madhumita, P. Guha and A. Nag, Bio-actives of betel leaf (Piper betle L.): A comprehensive review on extraction, isolation, characterization, and biological activity, *Phytother. Res.*, 2020, **34**(10), 2609–2627, DOI: **10.1002/ptr.6715**.

19 B. Patra, R. Meena, R. Rosalin, M. Singh, R. Paulraj, R. K. Ekka and S. N. Pradhan, Untargeted Metabolomics in Piper betle Leaf Extracts to Discriminate the Cultivars of Coastal Odisha, India, *Appl. Biochem. Biotechnol.*, 2022, **194**(10), 4362–4376, DOI: **10.1007/s12010-022-03873-0**.

20 D. Choudhary and R. K. Kale, Antioxidant and non-toxic properties of Piper betle leaf extract: in vitro and in vivo studies, *Phytother. Res.*, 2002, **16**(5), 461–466, DOI: **10.1002/ptr.1015**.

21 R. Murugan, The paradox of paan: ultural significance, carcinogenic risks, and betel leaf's anti-cancer properties, *Nat. Prod. Res.*, 2024, **17**, 1–2, DOI: **10.1080/14786419.2024.2368747**.

22 B. Patra, S. K. Deep, R. Rosalin and S. N. Pradhan, Flavored Food Additives on the Leaves of Piper betle L.: A Human Health Perspective, *Appl. Biochem. Biotechnol.*, 2022, **194**(10), 4439–4461, DOI: **10.1007/s12010-022-03912-w**.

23 N. T. Nguyen, T. H. Vu and V. H. Bui, Antibacterial and Antifungal Fabrication of Natural Lining Leather Using Bio-Synthesized Silver Nanoparticles from Piper Betle L. Leaf Extract, *Polymers*, 2023, **15**(12), 2634, DOI: **10.3390/polym15122634**.

24 S. Khan, S. Singh, S. Gaikwad, N. Nawani, M. Junnarkar and S. V. Pawar, Optimization of process parameters for the synthesis of silver nanoparticles from Piper betle leaf aqueous extract, and evaluation of their antiphytofungal activity, *Environ. Sci. Pollut. Res. Int.*, 2020, **27**(22), 27221–27233, DOI: **10.1007/s11356-019-05239-2**.

25 R. Shanmuganathan, N. D. Nguyen and M. M. Al-Ansari, Synthesis of zero valent copper/iron nanoparticles using Piper betle leaves for the removal of pharmaceutical contaminant atorvastatin, *Environ. Res.*, 2024, **257**, 119334, DOI: **10.1016/j.envres.2024.119334**.

26 T. Gur, I. Meydan, H. Seckin, M. Bekmezci and F. Sen, Green synthesis, characterization and bioactivity of biogenic zinc oxide nanoparticles, *Environ. Res.*, 2022, **204**(Pt A), 111897, DOI: **10.1016/j.envres.2021.111897**.

27 S. S. Rad, A. M. Sani and S. Mohseni, Biosynthesis, characterization and antimicrobial activities of zinc oxide nanoparticles from leaf extract of Mentha pulegium (L.), *Microb. Pathog.*, 2019, **131**, 239–245, DOI: **10.1016/j.micpath.2019.04.022**.

28 A. H. Teuschl, M. van Griensven and H. Redl, Sericin removal from raw Bombyx mori silk scaffolds of high hierarchical order, *Tissue Eng., Part C*, 2014, **20**(5), 431–439, DOI: **10.1089/ten.TEC.2013.0278**.

29 G. Carissimi, A. A. Lozano-Pérez, M. G. Montalbán, S. D. Aznar-Cervantes, J. L. Cenis and G. Víllora, Revealing the Influence of the Degumming Process in the Properties of Silk Fibroin Nanoparticles, *Polymers*, 2019, **11**(12), 2045, DOI: **10.3390/polym11122045**.

30 K. Karthikeyan, S. Sekar, M. P. Devi, S. Inbasekaran, C. H. Lakshminarasaiah and T. P. Sastry, Fabrication of novel biofibers by coating silk fibroin with chitosan impregnated with silver nanoparticles, *J. Mater. Sci.: Mater. Med.*, 2011, **22**(12), 2721–2726, DOI: **10.1007/s10856-011-4462-9**.

31 G. Greco, H. Mirbaha, B. Schmuck, A. Rising and N. M. Pugno, Artificial and natural silk materials have high mechanical property variability regardless of sample size, *Sci. Rep.*, 2022, **12**(1), 3507, DOI: **10.1038/s41598-022-07212-5**.

32 M. M. Joseph, N. Hari, R. K. Pillai, A. J. Nair and T. S. Therakathinal, Galactoxyloglucan Endowed Biogenic Nanoimmunobiotics Arrests Microbial Growth and Elicits Antitumor Immunity, *ACS Appl. Bio Mater.*, 2020, **3**(2), 801–814, DOI: **10.1021/acsabm.9b00834**.

33 M. A. Simpson and J. J. Gozzo, Spectrophotometric determination of lymphocyte mediated sheep red blood cell hemolysis in vitro, *J. Immunol. Methods*, 1978, **21**(1–2), 159–165, DOI: **10.1016/0022-1759(78)90232-6**.

34 J. B. Nair, M. M. Joseph, S. Mohapatra, M. Safeera, S. Ghosh, T. T. Sreelekha and K. K. Maiti, A Dual-Targeting Octaguanidine-Doxorubicin Conjugate Transporter for Inducing Caspase-Mediated Apoptosis on Folate-Expressing Cancer Cells, *ChemMedChem*, 2016, **11**(7), 702–712, DOI: **10.1002/cmdc.201600029**.

35 S. R. Aravind, M. M. Joseph, S. K. George, K. V. Dileep, S. Varghese, A. Rose-James, P. Balaram, C. Sadasivan and T. T. Sreelekha, TRAIL-based tumor sensitizing galactoxyloglucan, a novel entity for targeting apoptotic machinery, *Int. J. Biochem. Cell Biol.*, 2015, **59**, 153–166, DOI: **10.1016/j.biocel.2014.11.019**.

36 A. Lagashetty and S. K. Ganiger, Shashidhar. Synthesis, characterization and antibacterial study of Ag-Au Bi-metallic nanocomposite by bioreduction using piper betle leaf extract, *Heliyon*, 2019, **5**(12), e02794, DOI: **10.1016/j.heliyon.2019.e02794**.

37 W. Muhammad, N. Ullah, M. Haroon and B. H. Abbasi, Optical, morphological and biological analysis of zinc oxide nanoparticles (ZnO NPs) using Papaver somniferum L, *RSC Adv.*, 2019, **9**(51), 29541–29548, DOI: **10.1039/c9ra04424h**.

38 D. Cao, S. Gong, X. Shu, D. Zhu and S. Liang, Preparation of ZnO Nanoparticles with High Dispersibility Based on Oriented Attachment (OA) Process, *Nanoscale Res. Lett.*, 2019, **14**(1), 210, DOI: **10.1186/s11671-019-3038-3**.

39 N. Sizochenko, A. Mikolajczyk, M. Syzochenko, T. Puzyn and J. Leszczynski, Zeta potentials (ζ) of metal oxide nanoparticles: A meta-analysis of experimental data and a predictive neural networks modeling, *NanoImpact*, 2021, **22**, 100317, DOI: **10.1016/j.impact.2021.100317**.

40 V. Maulidya, A. N. Hasanah, L. Rijai and M. Muchtaridi, Quality Control and Authentication of Black Betel Leaf Extract (Piper acre Blume) from East Kalimantan as an Antimicrobial Agent Using a Combination of High-Performance Liquid Chromatography and Chemometric Fourier Transform Infrared, *Molecules*, 2023, **28**(15), 5666, DOI: **10.3390/molecules28155666**.

41 S. Ling, Z. Qi, D. P. Knight, Z. Shao and X. Chen, Synchrotron FTIR microspectroscopy of single natural silk fibers, *Biomacromolecules*, 2011, **12**(9), 3344–3349, DOI: **10.1021/bm2006032**.

42 M. Hasannasab, J. Nourmohammadi, M. M. Dehghan and A. Ghaee, Immobilization of bromelain and ZnO nanoparticles on silk fibroin nanofibers as an antibacterial and anti-inflammatory burn dressing, *Int. J. Pharm.*, 2021, **610**, 121227, DOI: **10.1016/j.ijpharm.2021.121227**.

43 H. Sogawa, K. Nakano, A. Tateishi, K. Tajima and K. Numata, Surface Analysis of Native Spider Draglines by FE-SEM and XPS, *Front. Bioeng. Biotechnol.*, 2020, **8**, 231, DOI: **10.3389/fbioe.2020.00231**.

44 I. H. Makrygiannis, A. K. Nikolaidis, I. Tilaveridis, A. D. Kouvelas, I. N. Lykakis and G. Venetis, Coated sutures for use in oral surgery: a comprehensive review, *Clin. Oral Invest.*, 2025, **29**(2), 109, DOI: **10.1007/s00784-025-06176-w**.

45 Y. Hao, Y. Wang, L. Zhang, F. Liu, Y. Jin, J. Long, S. Chen, G. Duan and H. Yang, Advances in antibacterial activity of zinc oxide nanoparticles against Staphylococcus aureus, *Biomed. Rep.*, 2024, **21**(5), 161, DOI: **10.3892/br.2024.1849**.

46 S. P. Dhas, S. Anbarasan, A. Mukherjee and N. Chandrasekaran, Biobased silver nanocolloid coating on silk fibers for prevention of post-surgical wound infections, *Int. J. Nanomed.*, 2015, **10**(1), 159–170, DOI: **10.2147/IJN.S82211**.

47 M. Cestari, V. Muller, J. H. Rodrigues, C. V. Nakamura, A. F. Rubira and E. C. Muniz, Preparing silk fibroin nanofibers through electrospinning: further heparin immobilization toward hemocompatibility improvement, *Biomacromolecules*, 2014, **15**(5), 1762–1767, DOI: **10.1021/bm500132g**.

48 E. B. Byun, N. Y. Sung, J. H. Kim, J. I. Choi, T. Matsui, M. W. Byun and J. W. Lee, Enhancement of anti-tumor activity of gamma-irradiated silk fibroin via immunomodulatory effects, *Chem.-Biol. Interact.*, 2010, **186**(1), 90–95, DOI: **10.1016/j.cbi.2010.03.032**.

49 A. B. Mousa, R. Moawad, Y. Abdallah, M. Abdel-Rasheed and A. M. A. Zaher, Zinc Oxide Nanoparticles Promise Anticancer and Antibacterial Activity in Ovarian Cancer, *Pharm. Res.*, 2023, **40**(10), 2281–2290, DOI: **10.1007/s11095-023-03505-0**.

50 M. Premanathan, K. Karthikeyan, K. Jeyasubramanian and G. Manivannan, Selective toxicity of ZnO nanoparticles toward Gram-positive bacteria and cancer cells by apoptosis through lipid peroxidation, *Nanomedicine*, 2011, **7**(2), 184–192, DOI: **10.1016/j.nano.2010.10.001**.

51 K. M. Reddy, K. Feris, J. Bell, D. G. Wingett, C. Hanley and A. Punnoose, Selective toxicity of zinc oxide nanoparticles to prokaryotic and eukaryotic systems, *Appl. Phys. Lett.*, 2007, **90**(213902), 2139021–2139023, DOI: **10.1063/1.2742324**.

52 R. K. Shukla, V. Sharma, A. K. Pandey, S. Singh, S. Sultana and A. Dhawan, ROS-mediated genotoxicity induced by titanium dioxide nanoparticles in human epidermal cells, *Toxicol. In Vitro*, 2011, **25**(1), 231–241, DOI: **10.1016/j.tiv.2010.11.008**.

53 H. Yang, C. Liu, D. Yang, H. Zhang and Z. Xi, Comparative study of cytotoxicity, oxidative stress and genotoxicity induced by four typical nanomaterials: the role of particle size, shape and composition, *J. Appl. Toxicol.*, 2009, **29**(1), 69–78, DOI: **10.1002/jat.1385**.